

Search for proton decay via $p \rightarrow e^+\eta$ and $p \rightarrow \mu^+\eta$ with a 0.37 Mton-year exposure of Super-Kamiokande

N. Taniuchi,^{49,*} K. Abe,^{1,50} S. Abe,¹ Y. Asaoka,¹ C. Bronner,¹ M. Harada,¹ Y. Hayato,^{1,50} K. Hiraide,^{1,50} K. Hosokawa,¹ K. Ieki,^{1,50} M. Ikeda,^{1,50} J. Kameda,^{1,50} Y. Kanemura,¹ R. Kaneshima,¹ Y. Kashiwagi,¹ Y. Kataoka,^{1,50} S. Miki,¹ S. Mine,^{1,7} M. Miura,^{1,50} S. Moriyama,^{1,50} M. Nakahata,^{1,50} S. Nakayama,^{1,50} Y. Noguchi,¹ G. Pronost,¹ K. Okamoto,¹ K. Sato,¹ H. Sekiya,^{1,50} H. Shiba,¹ K. Shimizu,¹ M. Shiozawa,^{1,50} Y. Sonoda,¹ Y. Suzuki,¹ A. Takeda,^{1,50} Y. Takemoto,¹ A. Takenaka,¹ H. Tanaka,^{1,50} S. Watanabe,¹ T. Yano,¹ T. Kajita,^{2,50,23} K. Okumura,^{2,50} T. Tashiro,² T. Tomiya,² X. Wang,² S. Yoshida,² G. D. Megias,³ P. Fernandez,⁴ L. Labarga,⁴ N. Ospina,⁴ B. Zaldivar,⁴ B. W. Pointon,^{6,55} E. Kearns,^{5,50} J. Mirabito,⁵ J. L. Raaf,⁵ L. Wan,⁵ T. Wester,⁵ J. Bian,⁷ N. J. Griskevich,⁷ W. R. Kropp,^{7,†} S. Locke,^{7,50} M. B. Smy,^{7,50} H. W. Sobel,^{7,50} V. Takhistov,^{7,25} A. Yankelevich,⁷ J. Hill,⁸ M. C. Jang,⁹ J. Y. Kim,⁹ S. H. Lee,⁹ I. T. Lim,⁹ D. H. Moon,⁹ R. G. Park,⁹ B. S. Yang,⁹ B. Bodur,¹⁰ K. Scholberg,^{10,50} C. W. Walter,^{10,50} A. Beauchêne,¹¹ L. Bernard,¹¹ A. Coffani,¹¹ O. Drapier,¹¹ S. El Hedri,¹¹ A. Giampaolo,¹¹ Th. A. Mueller,¹¹ A. D. Santos,¹¹ P. Paganini,¹¹ R. Rogly,¹¹ T. Nakamura,¹² J. S. Jang,¹³ L. N. Machado,¹⁴ J. G. Learned,¹⁵ K. Choi,¹⁶ N. Iovine,¹⁶ S. Cao,¹⁷ L. H. V. Anthony,¹⁸ D. Martin,¹⁸ N. W. Prouse,¹⁸ M. Scott,¹⁸ A. A. Sztuc,¹⁸ Y. Uchida,¹⁸ V. Berardi,¹⁹ N. F. Calabria,¹⁹ M. G. Catanesi,¹⁹ E. Radicioni,¹⁹ A. Langella,²⁰ G. De Rosa,²⁰ G. Collazuol,²¹ M. Feltre,²¹ F. Jacob,²¹ M. Lamoureux,²¹ M. Mattiazzi,²¹ L. Ludovici,²² M. Gonin,²³ L. Périssé,²³ B. Quilain,²³ C. Fujisawa,²⁴ S. Horiuchi,²⁴ M. Kobayashi,²⁴ Y. M. Liu,²⁴ Y. Maekawa,²⁴ Y. Nishimura,²⁴ R. Okazaki,²⁴ R. Akutsu,²⁵ M. Friend,²⁵ T. Hasegawa,²⁵ T. Ishida,²⁵ T. Kobayashi,²⁵ M. Jakkapu,²⁵ T. Matsubara,²⁵ T. Nakadaira,²⁵ K. Nakamura,^{25,50} Y. Oyama,²⁵ A. Portocarrero Yrey,²⁵ K. Sakashita,²⁵ T. Sekiguchi,²⁵ T. Tsukamoto,²⁵ N. Bhuiyan,²⁶ T. Boschi,²⁶ G. T. Burton,²⁶ F. Di Lodovico,²⁶ J. Gao,²⁶ A. Goldsack,²⁶ T. Katori,²⁶ J. Migenda,²⁶ R. M. Ramsden,²⁶ M. Taani,²⁶ Z. Xie,²⁶ S. Zsoldos,^{26,50} Y. Kotsar,²⁷ H. Ozaki,²⁷ A. T. Suzuki,²⁷ Y. Takagi,²⁷ Y. Takeuchi,^{27,50} S. Yamamoto,²⁷ H. Zhong,²⁷ J. Feng,²⁸ L. Feng,²⁸ S. Han,²⁸ J. R. Hu,²⁸ Z. Hu,²⁸ M. Kawaue,²⁸ T. Kikawa,²⁸ M. Mori,²⁸ T. Nakaya,^{28,50} R. A. Wendell,^{28,50} K. Yasutome,²⁸ S. J. Jenkins,²⁹ N. McCauley,²⁹ P. Mehta,²⁹ A. Tarrant,²⁹ M. J. Wilking,³⁰ Y. Fukuda,³¹ Y. Itow,^{32,33} H. Menjo,³² K. Ninomiya,³² Y. Yoshioka,³² J. Lagoda,³⁴ M. Mandal,³⁴ P. Mijakowski,³⁴ Y. S. Prabhu,³⁴ J. Zalipska,³⁴ M. Jia,³⁵ J. Jiang,³⁵ C. K. Jung,³⁵ W. Shi,³⁵ C. Yanagisawa,^{35,‡} Y. Hino,³⁶ H. Ishino,³⁶ S. Ito,³⁶ H. Kitagawa,³⁶ Y. Koshio,^{36,50} W. Ma,³⁶ F. Nakanishi,³⁶ S. Sakai,³⁶ T. Tada,³⁶ T. Tano,³⁶ T. Ishizuka,³⁷ G. Barr,³⁸ D. Barrow,³⁸ L. Cook,^{38,50} S. Samani,³⁸ D. Wark,^{38,44} A. Holin,³⁹ F. Nova,³⁹ S. Jung,⁴⁰ J. Y. Yang,⁴⁰ J. Yoo,⁴⁰ J. E. P. Fannon,⁴¹ L. Kneale,⁴¹ M. Malek,⁴¹ J. M. McElwee,⁴¹ O. Stone,⁴¹ P. Stowell,⁴¹ M. D. Thiesse,⁴¹ L. F. Thompson,⁴¹ S. T. Wilson,⁴¹ H. Okazawa,⁴² S. M. Lakshmi,⁴³ S. B. Kim,⁴⁵ E. Kwon,⁴⁵ M. W. Lee,⁴⁵ J. W. Seo,⁴⁵ I. Yu,⁴⁵ A. K. Ichikawa,⁴⁶ K. D. Nakamura,⁴⁶ S. Tairafune,⁴⁶ K. Nishijima,⁴⁷ M. Koshiba,^{48,†} A. Eguchi,⁴⁹ S. Goto,⁴⁹ K. Iwamoto,⁴⁹ Y. Mizuno,⁴⁹ T. Muro,⁴⁹ K. Nakagiri,⁴⁹ Y. Nakajima,^{49,50} S. Shima,⁴⁹ E. Watanabe,⁴⁹ M. Yokoyama,^{49,50} P. de Perio,⁵⁰ S. Fujita,⁵⁰ C. Jesús-Valls,⁵⁰ K. Martens,⁵⁰ Ll. Marti,⁵⁰ K. M. Tsui,⁵⁰ M. R. Vagins,^{50,7} J. Xia,⁵⁰ S. Izumiyama,⁵¹ M. Kuze,⁵¹ R. Matsumoto,⁵¹ K. Terada,⁵¹ R. Asaka,⁵² M. Inomoto,⁵² M. Ishitsuka,⁵² H. Ito,⁵² T. Kinoshita,⁵² Y. Ommura,⁵² N. Shigeta,⁵² M. Shinoki,⁵² T. Sukanuma,⁵² K. Yamauchi,⁵² T. Yoshida,⁵² Y. Nakano,⁵³ J. F. Martin,⁵⁴ H. A. Tanaka,⁵⁴ T. Towstego,⁵⁴ R. Gaur,⁵⁵ V. Gousy-Leblanc,^{55,§} M. Hartz,⁵⁵ A. Konaka,⁵⁵ X. Li,⁵⁵ S. Chen,⁵⁶ Y. Wu,⁵⁶ B. D. Xu,⁵⁶ A. Q. Zhang,⁵⁶ B. Zhang,⁵⁶ M. Posiadala-Zezula,⁵⁷ S. B. Boyd,⁵⁸ R. Edwards,⁵⁸ D. Hadley,⁵⁸ M. Nicholson,⁵⁸ M. O'Flaherty,⁵⁸ B. Richards,⁵⁸ A. Ali,^{59,55} B. Jamieson,⁵⁹ S. Amanai,⁶⁰ A. Minamino,⁶⁰ G. Pintaudi,⁶⁰ S. Sano,⁶⁰ R. Sasaki,⁶⁰ R. Shibayama,⁶⁰ R. Shimamura,⁶⁰ S. Suzuki,⁶⁰ and K. Wada⁶⁰

(The Super-Kamiokande Collaboration)

¹Kamioka Observatory, Institute for Cosmic Ray Research, University of Tokyo, Kamioka, Gifu 506-1205, Japan

²Research Center for Cosmic Neutrinos, Institute for Cosmic Ray Research, University of Tokyo, Kashiwa, Chiba 277-8582, Japan

³Institute for Cosmic Ray Research, University of Tokyo, Kashiwa, Chiba 277-8582, Japan

⁴Department of Theoretical Physics, University Autonoma Madrid, 28049 Madrid, Spain

⁵Department of Physics, Boston University, Boston, MA 02215, USA

⁶Department of Physics, British Columbia Institute of Technology, Burnaby, BC, V5G 3H2, Canada

⁷Department of Physics and Astronomy, University of California, Irvine, Irvine, CA 92697-4575, USA

⁸Department of Physics, California State University, Dominguez Hills, Carson, CA 90747, USA

⁹Institute for Universe and Elementary Particles, Chonnam National University, Gwangju 61186, Korea

¹⁰Department of Physics, Duke University, Durham NC 27708, USA

¹¹Ecole Polytechnique, IN2P3-CNRS, Laboratoire Leprince-Ringuet, F-91120 Palaiseau, France

¹²Department of Physics, Gifu University, Gifu, Gifu 501-1193, Japan

- ¹³ GIST College, Gwangju Institute of Science and Technology, Gwangju 500-712, Korea
- ¹⁴ School of Physics and Astronomy, University of Glasgow, Glasgow, Scotland, G12 8QQ, United Kingdom
- ¹⁵ Department of Physics and Astronomy, University of Hawaii, Honolulu, HI 96822, USA
- ¹⁶ Center for Underground Physics, Institute for Basic Science (IBS), Daejeon, 34126, Korea
- ¹⁷ Institute For Interdisciplinary Research in Science and Education, ICISE, Quy Nhon, 55121, Vietnam
- ¹⁸ Department of Physics, Imperial College London, London, SW7 2AZ, United Kingdom
- ¹⁹ Dipartimento Interuniversitario di Fisica, INFN Sezione di Bari and Università e Politecnico di Bari, I-70125, Bari, Italy
- ²⁰ Dipartimento di Fisica, INFN Sezione di Napoli and Università di Napoli, I-80126, Napoli, Italy
- ²¹ Dipartimento di Fisica, INFN Sezione di Padova and Università di Padova, I-35131, Padova, Italy
- ²² INFN Sezione di Roma and Università di Roma “La Sapienza”, I-00185, Roma, Italy
- ²³ International Laboratory for Astrophysics, Neutrino and Cosmology Experiment, Kashiwa, Chiba 277-8582, Japan
- ²⁴ Department of Physics, Keio University, Yokohama, Kanagawa, 223-8522, Japan
- ²⁵ High Energy Accelerator Research Organization (KEK), Tsukuba, Ibaraki 305-0801, Japan
- ²⁶ Department of Physics, King’s College London, London, WC2R 2LS, UK
- ²⁷ Department of Physics, Kobe University, Kobe, Hyogo 657-8501, Japan
- ²⁸ Department of Physics, Kyoto University, Kyoto, Kyoto 606-8502, Japan
- ²⁹ Department of Physics, University of Liverpool, Liverpool, L69 7ZE, United Kingdom
- ³⁰ School of Physics and Astronomy, University of Minnesota, Minneapolis, MN 55455, USA
- ³¹ Department of Physics, Miyagi University of Education, Sendai, Miyagi 980-0845, Japan
- ³² Institute for Space-Earth Environmental Research, Nagoya University, Nagoya, Aichi 464-8602, Japan
- ³³ Kobayashi-Maskawa Institute for the Origin of Particles and the Universe, Nagoya University, Nagoya, Aichi 464-8602, Japan
- ³⁴ National Centre For Nuclear Research, 02-093 Warsaw, Poland
- ³⁵ Department of Physics and Astronomy, State University of New York at Stony Brook, NY 11794-3800, USA
- ³⁶ Department of Physics, Okayama University, Okayama, Okayama 700-8530, Japan
- ³⁷ Media Communication Center, Osaka Electro-Communication University, Neyagawa, Osaka, 572-8530, Japan
- ³⁸ Department of Physics, Oxford University, Oxford, OX1 3PU, United Kingdom
- ³⁹ Rutherford Appleton Laboratory, Harwell, Oxford, OX11 0QX, UK
- ⁴⁰ Department of Physics, Seoul National University, Seoul 151-742, Korea
- ⁴¹ Department of Physics and Astronomy, University of Sheffield, S3 7RH, Sheffield, United Kingdom
- ⁴² Department of Informatics in Social Welfare, Shizuoka University of Welfare, Yaizu, Shizuoka, 425-8611, Japan
- ⁴³ August Chelkowski Institute of Physics, University of Silesia in Katowice, 75 Pułku Piechoty 1, 41-500 Chorzów, Poland
- ⁴⁴ STFC, Rutherford Appleton Laboratory, Harwell Oxford, and Daresbury Laboratory, Warrington, OX11 0QX, United Kingdom
- ⁴⁵ Department of Physics, Sungkyunkwan University, Suwon 440-746, Korea
- ⁴⁶ Department of Physics, Faculty of Science, Tohoku University, Sendai, Miyagi, 980-8578, Japan
- ⁴⁷ Department of Physics, Tokai University, Hiratsuka, Kanagawa 259-1292, Japan
- ⁴⁸ The University of Tokyo, Bunkyo, Tokyo 113-0033, Japan
- ⁴⁹ Department of Physics, University of Tokyo, Bunkyo, Tokyo 113-0033, Japan
- ⁵⁰ Kavli Institute for the Physics and Mathematics of the Universe (WPI), The University of Tokyo Institutes for Advanced Study, University of Tokyo, Kashiwa, Chiba 277-8583, Japan
- ⁵¹ Department of Physics, Tokyo Institute of Technology, Meguro, Tokyo 152-8551, Japan
- ⁵² Department of Physics, Faculty of Science and Technology, Tokyo University of Science, Noda, Chiba 278-8510, Japan
- ⁵³ Faculty of Science, University of Toyama, Toyama City, Toyama 930-8555, Japan
- ⁵⁴ Department of Physics, University of Toronto, ON, M5S 1A7, Canada
- ⁵⁵ TRIUMF, 4004 Wesbrook Mall, Vancouver, BC, V6T2A3, Canada
- ⁵⁶ Department of Engineering Physics, Tsinghua University, Beijing, 100084, China
- ⁵⁷ Faculty of Physics, University of Warsaw, Warsaw, 02-093, Poland
- ⁵⁸ Department of Physics, University of Warwick, Coventry, CV4 7AL, UK
- ⁵⁹ Department of Physics, University of Winnipeg, MB R3J 3L8, Canada
- ⁶⁰ Department of Physics, Yokohama National University, Yokohama, Kanagawa, 240-8501, Japan

(Dated: October 1, 2024)

A search for proton decay into e^+/μ^+ and a η meson has been performed using data from a 0.373 Mton-year exposure (6050.3 live days) of Super-Kamiokande. Compared to previous searches this work introduces an improved model of the intranuclear η interaction cross section, resulting in a factor of two reduction in uncertainties from this source and $\sim 10\%$ increase in signal efficiency. No significant data excess was found above the expected number of atmospheric neutrino background events resulting in no indication of proton decay into either mode. Lower limits on the proton partial lifetime of 1.4×10^{34} years for $p \rightarrow e^+\eta$ and 7.3×10^{33} years for $p \rightarrow \mu^+\eta$ at the 90% C.L. were set. These limits are around 1.5 times longer than our previous study and are the most stringent to date.

* Present Address: Department of Physics, Cavendish Laboratory,

University of Cambridge, Cambridge, CB3 0HE, United King-

I. INTRODUCTION

While the Standard Model of particle physics successfully explains most experimental data with exceptional precision it is not a complete description of nature. Notably it does not offer sufficient explanations for the observed quantization of electric charge nor for the convergence of the electromagnetic, weak, and strong interaction couplings at high energy scales. To address those questions, Grand Unified Theories (GUTs) extend the Standard Model by incorporating its $SU(3)_c \times SU(2)_L \times U(1)_Y$ gauge symmetry into larger symmetry groups, such as $SU(5)$ [1] or $SO(10)$ [2]. Most GUTs permit new interactions where leptons and quarks transform into each other and thereby induce baryon-number-violating proton decays with considerably long lifetimes. Though the gauge couplings in GUTs are estimated to unify near $\sim 10^{16}$ GeV, an energy too high to be reached by accelerators, the observation of proton decay would be an experimental verification of such high energy theories.

While the predicted lifetime and products of proton decay depend on the GUT model, many are expected to be observable with the Super-Kamiokande (SK) experiment. The $p \rightarrow l^+ \pi^0$ ($l = e^+, \mu^+$) and $p \rightarrow \bar{\nu} K^+$ modes, for example, are favored decays in many nonsupersymmetric and TeV-scale supersymmetric GUTs [3, 4], both of which have been tested at SK. No significant signal has been observed in either [5, 6] and the world's most stringent limits, corresponding to lifetimes of the order of 10^{34} years, have been set. The $p \rightarrow l^+ \pi^0$ modes are readily probed at SK due to its large size and highly efficient detection of the decay products; two γ -rays from the π^0 decay and a single l^+ , which is predicted to be above Cherenkov threshold, can be observed clearly. However, some models [7–10] suggest that the decay rates of channels with heavy non-strange mesons (η, ρ, ω) are comparable in magnitude to those with pions. In particular, the $p \rightarrow l^+ \eta$ decay generates a similar signal to that from $p \rightarrow l^+ \pi^0$, where the η meson mainly decays into two γ -rays, resulting in a relatively high detection efficiency. It is essential to search for such possibilities as well, since it is not known which proton decay mode is dominant and since the observation of multiple modes can be used to determine the GUT gauge group.

Our most recent search for the $p \rightarrow l^+ \eta$ decay used 0.316 Mton-years of SK data [11] and concluded with no positive observations, setting lower limits on the partial lifetime of $\tau/B(p \rightarrow e^+ \eta) > 1.0 \times 10^{34}$ years and

$\tau/B(p \rightarrow \mu^+ \eta) > 4.7 \times 10^{33}$ years at 90% confidence level (C.L.). This paper describes improved searches for these two modes using a total exposure of 0.373 Mton-years, corresponding to a $\sim 18\%$ increase in exposure from the SK-IV period. The present work additionally includes an improved estimation of the intranuclear η interaction cross sections and their accompanying uncertainties.

II. SUPER-KAMIOKANDE DETECTOR

Super-Kamiokande is a large water Cherenkov detector located 1,000 m beneath Mt. Ikenoyama (2700 m.w.e.), in the Kamioka-mine in Hida-city, Gifu Prefecture, Japan. The detector is a cylindrical stainless-steel tank with a 39.3 m diameter and a 41.4 m height that is filled with 50 ktons of ultrapure water. It is separated into two sections: the inner detector (ID) and the outer detector (OD). The ID forms the main target mass and has a diameter of 33.8 m and a height of 36.2 m. It is viewed by more than 11,000 20-inch photomultiplier tubes (PMTs), which face inwards. On the other hand, the primary functions of the OD are to veto cosmic ray muons and to serve as a shield against radiation coming from the rock around the detector. The OD is a 2 m-thick cylindrical annulus viewed by 1,885 outward-facing 8-inch PMTs. The detector is described in more detail in [12, 13].

Up until 2018, the SK data are divided into four periods: SK-I, II, III, and IV. The SK-I period started on April 1st 1996 and ran with a photocathode coverage of 40% until July 2001. Due to a chain reaction implosion in November 2001 the SK-II period was operated with 5,182 ID PMTs, corresponding to 19% photocathode coverage, from October 2002 to October 2005. After replenishing the missing PMTs, data taking started again at the nominal 40% coverage from June 2006 to September 2008 (SK-III). In September 2008, new front-end electronics [14] were installed to start the SK-IV period, which ended in May 2018. This upgrade allows events to be recorded with no dead time, thereby enabling the detection of γ -rays from neutron capture on a hydrogen nucleus. In this study, all available data from SK-I to SK-IV are utilized. A total 0.373 Mton-year exposure from 91.5, 49.1, 31.8, and 199.4 kton-years of the SK-I, II, III, and IV periods, respectively, is used.

III. SIMULATION

A. Proton Decay MC

Dedicated proton decay Monte Carlo (MC) samples for $p \rightarrow l^+ \eta$ modes are generated for the estimation of signal detection efficiencies. Inside SK, proton decay events are assumed to occur both in hydrogen nuclei as free protons and in oxygen nuclei as bound protons in a ratio of one to four in the H_2O molecule. Protons are considered to decay with the same probability regardless of

dom

† Deceased.

‡ also at BMCC/CUNY, Science Department, New York, New York, 1007, USA.

§ also at University of Victoria, Department of Physics and Astronomy, PO Box 1700 STN CSC, Victoria, BC V8W 2Y2, Canada.

their initial states. The $p \rightarrow l^+ \eta$ proton decay events are treated as two body decays. While hydrogen nuclei (free protons) are stationary and do not interact with other nucleons, bound protons in oxygen nuclei are subject to the effects of Fermi motion, nuclear binding energy, and correlated momentum effects with surrounding nucleons. Furthermore, η mesons emitted by proton decays can interact with nucleons, being absorbed or scattered, prior to exiting the nucleus. The decaying proton's position in the nucleus is given by the Woods-Saxon nuclear density model [15].

The Fermi motion and nuclear binding energy in ^{16}O are simulated based on electron scattering experiments on ^{12}C [16]. The ^{16}O nuclear binding energies are 39.0 MeV for the s -state and 15.5 MeV for the p -state protons. In the simulation, an effective mass of the proton is introduced by subtracting the binding energy from the proton rest mass. Decaying protons can be affected by the other nucleons in the same ^{16}O nucleus due to wavefunction overlap (correlated decay). This effect is predicted to occur in $\sim 10\%$ of protons [17], resulting in an effective three-body decay with a recoiling nucleon, which carries away momentum and produces a tail in the lower mass region of the proton mass distribution. Finally, the η mesons generated by bound protons in the ^{16}O nucleus can interact with nucleons while escaping from the nucleus (η nuclear effect, presented in detail in Section III B). Each of these effects alter final kinematics of the decay particles relative to those from free proton decays.

B. η Nuclear Effect

η mesons emitted from ^{16}O proton decays can interact with nucleons while travelling through the nucleus and form several baryon resonance states in the process. Of these, the $S_{11}(1535)$ resonance state has been studied exclusively due to the property that it exists slightly above the $\eta - N$ production threshold, thereby providing a large branching ratio for $S_{11}(1535) \rightarrow N + \eta$ [18, 19]. Therefore, in this study the η nuclear effect is evaluated through $S_{11}(1535)$ resonance state.

Since this nuclear effect plays a crucial role in proton decay searches due to its impact on the number of observable η mesons, it is important to derive a reliable estimation of the cross section for this reaction. In our previous study [20], the cross section of the η nuclear effect, σ_{nuc} , was calculated with the Breit-Wigner formula [21]. Experimental η meson photoproduction data [19] was then used to assess its uncertainty: The measured differential cross section for the η photoproduction reaction $d\sigma_{\eta\text{photo}}/dp$ [19] was compared with the simulated value from the NEUT interaction generator [22, 23], which includes the calculated η nuclear effect cross section.

This study, on the other hand, additionally makes use of η absorption cross section measurement, σ_{abs} , which was independently deduced from total η photoproduction

data on various targets [19]. Here σ_{nuc} and its uncertainty are estimated by adopting the least χ^2 method to fit functional forms to the measured $d\sigma_{\eta\text{photo}}/dp$ and σ_{abs} from [19]. We assume that $\sigma_{\text{abs}} \sim \sigma_{\text{nuc}}$, with the difference between them coming from the inclusion of elastic scattering and multi-step interaction effects. Both are expected to be minor, inducing only to a few percent difference as discussed in [19].

We adopt an exponential parameterisation for σ_{nuc} given by $\sigma_{\text{nuc}} = ae^{-bp_\eta}$, where a and b (≥ 0) are to be determined by the fit. Here p_η is the momentum of the η meson in the laboratory frame. This form is then propagated through NEUT (version 5.4.0) to calculate $d\sigma_{\eta\text{photo}}/dp$ as a function of a and b . These parameters are varied during a simultaneous fit to both the η absorption (Figure 1) and photoproduction cross section data (Figure 2) to determine the most compatible cross section form.

Figure 1 shows the measured σ_{nuc} (σ_{abs}) as well as our estimations at the best fit (a [mb], b [c/MeV]) = (46, 0.0023) and for parameters allowed at 1σ . Similarly, Figure 2 shows the result for the $d\sigma_{\eta\text{photo}}/dp$ cross section. The additional 6% systematic errors on the measured data points are not shown in the figures. Compared to our previous parameterisation, shown as the dotted line in both figures, generally the data are better described by the new parameterisation. This improved σ_{nuc} estimation reduces the systematic error by up to 65% compared to the previous analysis as is described in Section VI A.

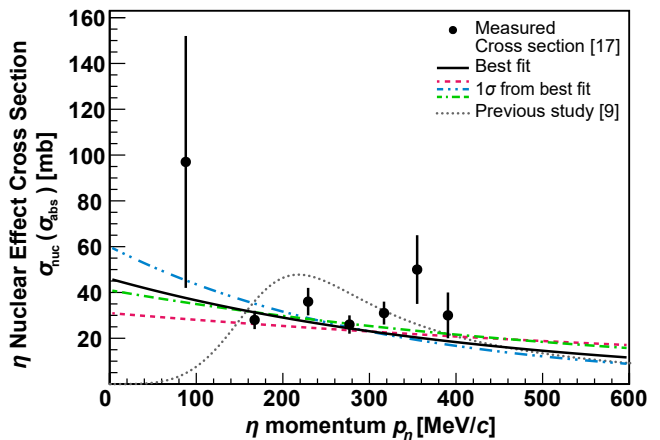


FIG. 1. Measured η absorption cross section, σ_{abs} , and fitted η nuclear effect cross section, σ_{nuc} . Experimental data for σ_{abs} from the Mainz experiment [19] are shown as the black circles with statistical errors only. The black solid line shows the fitted σ_{nuc} at the best fit parameters (a [mb], b [c/MeV]) = (46, 0.0023), while the red, green, and blue lines stand for that with representative parameters allowed at $\pm 1\sigma$, (a [mb], b [c/MeV]) = (31, 0.0010), (41, 0.0016), and (60, 0.0032), respectively. The dashed line shows σ_{nuc} from the previous analysis [11], which was calculated according to the Breit-Wigner formula.

C. Atmospheric ν MC

Backgrounds in the analysis are estimated using simulated atmospheric neutrino events corresponding to a 500-year exposure of the detector for each SK period. The atmospheric neutrino flux used in the simulation is taken from the Honda calculation [24, 25] and interactions are generated using the cross section models in NEUT [22], with updates described in [26]. Events with neutral pions, which are the dominant background in the present analysis, are subject to interactions with nucleons in the ^{16}O nucleus in a manner similar to the η nuclear effect. Pions can be scattered, absorbed, or charge exchanged (π nuclear effect). The cross sections for each of the processes are calculated by the NEUT cascade model [22, 27] with data from various $\pi - (p, n)$ and $\pi - N$ scattering experiments [28]. Uncertainties on these processes are important error sources in the present measurement. Meson production from atmospheric neutrino interactions in water, including π and η , are simulated in NEUT by the Rein-Sehgal Model [29]. More detailed information on the neutrino interaction and detector model are presented in [26].

IV. DATA REDUCTION AND EVENT RECONSTRUCTION

In this study data from a total exposure of 0.373 Mton-years and corresponding to 6050.3 live days is anal-

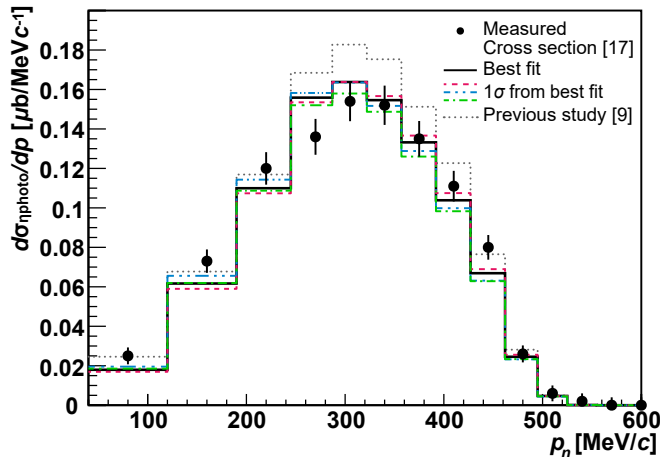


FIG. 2. Measured and simulated differential η photoproduction cross sections $d\sigma_{\eta\text{photo}}/dp$. Data from the Mainz experiment [19] are shown as the black circles with statistical errors only. The black solid line shows the $d\sigma_{\eta\text{photo}}/dp$ calculated using the best fit parameters (a [mb], b [c/MeV]) = (46, 0.0023) for σ_{nuc} , while the red, green, and blue lines stand for that with representative parameters allowed at $\pm 1\sigma$, (a [mb], b [c/MeV]) = (31, 0.0010), (41, 0.0016), and (60, 0.0032), respectively. The dashed line shows σ_{nuc} from the previous analysis [11].

ysed. This analysis uses only Fully Contained (FC) events, whose reconstructed vertices and all visible particles are contained within the ID fiducial volume. The fiducial volume is defined as the region 2 m away from the top, bottom, and barrel walls of the ID and corresponds to a 22.5 kton mass. These FC events are extracted during multiple reduction steps by algorithms identical to those applied in atmospheric neutrino studies and other nucleon decay searches [5, 11, 26]. After reduction, events are required to have vertices within the fiducial volume, with visible energies greater than 30 MeV, and with no cluster of OD PMTs with more than 16 hits.

Reconstruction processes are applied to all FC events to determine the event kinematic parameters, such as the number of Cherenkov rings, their momenta, and their particle type (PID). The APfit reconstruction [30, 31] is used in this analysis, as in the other atmospheric neutrino analyses and nucleon decay searches, and is applied to both data and MC events. The reconstruction starts by determining the vertex location using the point in the ID that maximizes the peak of the residual timing distribution assuming all light arriving at the PMTs originated from that point. Next, the direction and the edge of the most energetic Cherenkov ring are estimated from the angular distribution of the observed charge as a function of the opening angle. A ring pattern recognition algorithm based on the Hough transformation [32] is then used to search for additional Cherenkov rings. Each ring is classified as either a showering particle (e^\pm , γ) or a non-showering particle (μ^\pm , π^\pm) according to its hit pattern and opening angle. While the former creates a blurred ring pattern due to the induced electromagnetic shower and multiple scattering of particles therein, the latter shows a sharper ring edge. The momentum of each ring is evaluated using the observed charge inside the 70° half-angle cone around the ring direction after accounting for light attenuation in water and the angular acceptance of the PMTs. Michel electrons are tagged by searching for hit clusters after the primary Cherenkov ring event.

When neutrons thermalize in the detector water and capture on a hydrogen nucleus, a 2.2 MeV γ -ray is emitted. Such γ -rays can be tagged in the SK-IV period (and later) with a dedicated algorithm described in [33]. The neutron tagging efficiency is estimated to be 25.2% with a false-positive rate of 1.8% based on atmospheric neutrino MC and AmBe calibration data. Since proton decay is expected to produce neutrons with a probability of less than 10% [34, 35], neutron tagging enables the removal of many atmospheric neutrino backgrounds and hence improves the sensitivity of this search.

In the event selection used below, the reconstructed total momentum, P_{tot} , the invariant mass, M_{tot} , and the

total energy E_{tot} are defined as follows:

$$P_{\text{tot}} = \left| \sum_{i=1}^{n_{\text{par}}} \mathbf{p}_i \right|, \quad (1)$$

$$E_{\text{tot}} = \sum_{i=1}^{n_{\text{par}}} \sqrt{m_i^2 + \mathbf{p}_i^2}, \quad (2)$$

$$M_{\text{tot}} = \sqrt{E_{\text{tot}}^2 - P_{\text{tot}}^2}. \quad (3)$$

Here m_i is the mass of the i -th particle of proton decay product, \mathbf{p}_i is the momentum of i -th particle (ring), and n_{par} is the number reconstructed particles.

The reconstructed invariant mass of the η meson, m_η , is similarly calculated by summing all the momenta and energies of the reconstructed particles identified as the products of the η decay. This identification is made by taking all the possible combinations of observed showering Cherenkov rings and selecting the combination whose invariant mass reconstructs closest to the rest mass of η meson.

V. EVENT SELECTION

The η meson has three dominant decay modes with a lifetime of 5×10^{-19} s: $\eta \rightarrow 2\gamma$ (branching ratio of 39%), $\eta \rightarrow 3\pi^0$ (branching ratio of 33%), and $\eta \rightarrow \pi^+\pi^-\pi^0$ (branching ratio of 23%). The former two modes are analysed in this study, whereas the last one is excluded due to its smaller branching ratio and poor detection efficiency in SK [20].

A. $\eta \rightarrow 2\gamma$ search

The event selection criteria for the search for $p \rightarrow e^+\eta$, $\eta \rightarrow 2\gamma$ and $p \rightarrow \mu^+\eta$, $\eta \rightarrow 2\gamma$ are defined as follows:

- (A1) There are three Cherenkov rings.
- (A2) All rings are showering for $p \rightarrow e^+\eta$ and one of the rings is non-showering for $p \rightarrow \mu^+\eta$.
- (A3) The reconstructed η mass satisfies $480 < M_\eta < 620 \text{ MeV}/c^2$.
- (A4) There is no tagged Michel electron for $p \rightarrow e^+\eta$ and one for $p \rightarrow \mu^+\eta$.
- (A5) The total momentum is $P_{\text{tot}} < 250 \text{ MeV}/c$ and the invariant mass satisfies $800 < M_{\text{tot}} < 1050 \text{ MeV}/c^2$.
- (A6) The total momentum P_{tot} is greater than or (A7) less than $100 \text{ MeV}/c$.
- (A8) There is no tagged neutron in the upper nor (A9) lower total momentum region for the SK-IV data.

Two signal boxes are defined by selections on the total momentum (A6 & A7): a lower signal box with $P_{\text{tot}} < 100 \text{ MeV}/c$ and an upper signal box with $100 \leq P_{\text{tot}} < 250 \text{ MeV}/c$ cuts. This separation is applied since the expected background rate in the $p_{\text{tot}} < 100 \text{ MeV}/c$ region is negligibly small ($\ll 0.1$ events in each SK period) and signal events in this region are primarily from the decay of free protons. Signal selection efficiencies and the expected number of atmospheric neutrino background events at each stage of the selection are shown in Fig. 3 and are summarized in Table I.

Efficiencies are evaluated using the number of proton decay MC events passing the selection criteria. Background events are estimated by applying the criteria to 500-year-equivalent atmospheric neutrino MC samples for each SK period (2000 years in total) and then normalizing by live time observed in data and reweighted based on the SK oscillation fit [26]. In this analysis, signal selection efficiencies have increased by $\sim 10\%$ compared to the previous analysis [11] due to the re-estimation of η nuclear effect as described in Section III B. The downward adjustment in σ_{nuc} around $p_\eta = 200 - 300 \text{ MeV}/c$ as shown in Fig. 1 results in an increase in the number of proton decay signal events whose η mesons have not been scattered nor absorbed, making them easier to detect.

The reconstructed momenta and mass cuts are especially significant in distinguishing proton decay signals from backgrounds as atmospheric neutrino events seldom produce isotropic event topologies; most neutrino-induced particles are emitted in the direction of the neutrino momentum. Selection (A5) reduces the number of expected background events to < 0.01 integrated over all SK periods for both the $p \rightarrow e^+\eta$ and $p \rightarrow \mu^+\eta$ searches in the lower signal box analysis (A9), while keeping the signal efficiency high.

Figure 4 shows the distribution of events passing the selection in the total mass and total momentum plane, but excluding cuts on those variables. One-dimensional distributions of these parameters are shown in Fig. 5 and Fig. 6 for the signal MC, the 2000-year atmospheric neutrino MC, and the integrated data from SK-I to SK-IV. All selection criteria except for those on the plotted variables are applied. Most of the free proton decay events populate the lower signal boxes ($P_{\text{tot}} < 100 \text{ MeV}/c$).

B. $\eta \rightarrow 3\pi^0$ search

The event selection criteria for the search for $p \rightarrow e^+\eta$, $\eta \rightarrow 3\pi^0$ and $p \rightarrow \mu^+\eta$, $\eta \rightarrow 3\pi^0$ are defined as follows:

- (B1) There are four or five Cherenkov rings.
- (B2) All rings are showering for $p \rightarrow e^+\eta$ and one of the rings is non-showering for $p \rightarrow \mu^+\eta$.
- (B3) The reconstructed η mass satisfies $400 < M_\eta < 700 \text{ MeV}/c^2$.

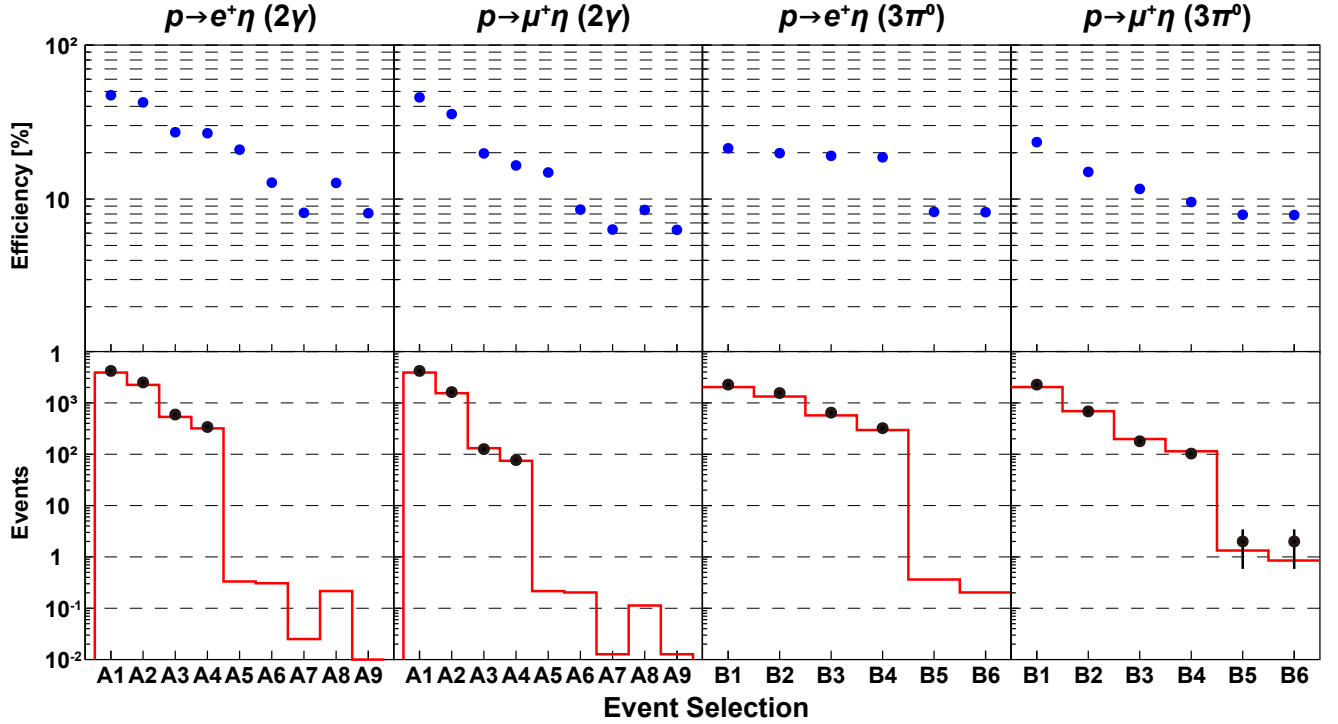


FIG. 3. The signal efficiencies (upper) and the number of expected backgrounds (lower, red histogram) and data candidates (lower, black circles) for $p \rightarrow e^+ \eta$ ($\eta \rightarrow 2\gamma$), $p \rightarrow \mu^+ \eta$ ($\eta \rightarrow 2\gamma$), $p \rightarrow e^+ \eta$ ($\eta \rightarrow 3\pi^0$), $p \rightarrow \mu^+ \eta$ ($\eta \rightarrow 3\pi^0$) searches from left to right. All the results from SK-I to SK-IV are combined. The event selection criteria are defined in Section V. The numbers of events of backgrounds and data candidates agree within 15% from cuts A1-A4 and B1-B4, which are well covered by systematic model variations.

TABLE I. Summary of the signal efficiencies, the number of expected background events and the number of candidate events from 91.5, 49.1, 31.8, and 199.9 kton-years exposures of the SK-I, SK-II, SK-III, and SK-IV periods, respectively. The errors on the background events are statistical uncertainties from 500 years of atmospheric neutrino MC for each SK period. The “upper” and “lower” in the $\eta \rightarrow 2\gamma$ searches stand for $100 \leq p_{\text{tot}} < 250$ MeV/c and $p_{\text{tot}} < 100$ MeV/c, respectively.

| SK period | Efficiency [%] | | | | Background [events] | | | | Candidate [events] | | | |
|----------------------------|----------------|------|------|------|---------------------|-------------------|-------------------|-------------------|--------------------|----|-----|----|
| | I | II | III | IV | I | II | III | IV | I | II | III | IV |
| $p \rightarrow e^+ \eta$ | | | | | | | | | | | | |
| (2γ , upper) | 13.9 | 11.9 | 12.9 | 12.2 | 0.08 ± 0.03 | 0.05 ± 0.01 | 0.03 ± 0.01 | 0.05 ± 0.03 | 0 | 0 | 0 | 0 |
| (2γ , lower) | 8.2 | 7.8 | 8.5 | 8.0 | 0.000 ± 0.006 | 0.004 ± 0.004 | 0.003 ± 0.003 | 0.000 ± 0.010 | 0 | 0 | 0 | 0 |
| ($3\pi^0$) | 8.4 | 8.4 | 7.7 | 8.4 | 0.06 ± 0.02 | 0.06 ± 0.02 | 0.03 ± 0.01 | 0.05 ± 0.03 | 0 | 0 | 0 | 0 |
| $p \rightarrow \mu^+ \eta$ | | | | | | | | | | | | |
| (2γ , upper) | 8.3 | 6.9 | 8.9 | 9.9 | 0.05 ± 0.02 | 0.04 ± 0.01 | 0.003 ± 0.003 | 0.03 ± 0.02 | 0 | 0 | 0 | 0 |
| (2γ , lower) | 6.3 | 5.6 | 6.3 | 7.1 | 0.008 ± 0.008 | 0.004 ± 0.004 | 0.000 ± 0.003 | 0.000 ± 0.010 | 0 | 0 | 0 | 0 |
| ($3\pi^0$) | 7.9 | 6.2 | 7.8 | 9.6 | 0.38 ± 0.05 | 0.17 ± 0.03 | 0.12 ± 0.02 | 0.17 ± 0.05 | 0 | 1 | 0 | 1 |

(B4) There is no tagged Michel electron for $p \rightarrow e^+ \eta$ and one for $p \rightarrow \mu^+ \eta$.

(B5) The total momentum is $P_{\text{tot}} < 150$ MeV/c for $p \rightarrow e^+ \eta$ and $P_{\text{tot}} < 250$ MeV/c for $p \rightarrow \mu^+ \eta$. The invariant mass satisfies $800 < M_{\text{tot}} < 1050$ MeV/c².

(B6) There is no tagged neutron for the SK-IV data.

The signal selection efficiencies and the expected number of atmospheric neutrino background events at each

step of the selection are shown in Fig. 3. In this decay mode the three neutral pions decay into six γ -rays and generate six Cherenkov rings. However, as the ring counting algorithm is only able to identify up to five rings, the condition on the number of rings is set to be four or five (B1). This results in a reduced ability to reconstruct the η mass and therefore the event selection window of η mass (B3) is set to be larger than in the $\eta \rightarrow 2\gamma$ search. The two-dimensional total mass and total momentum distri-

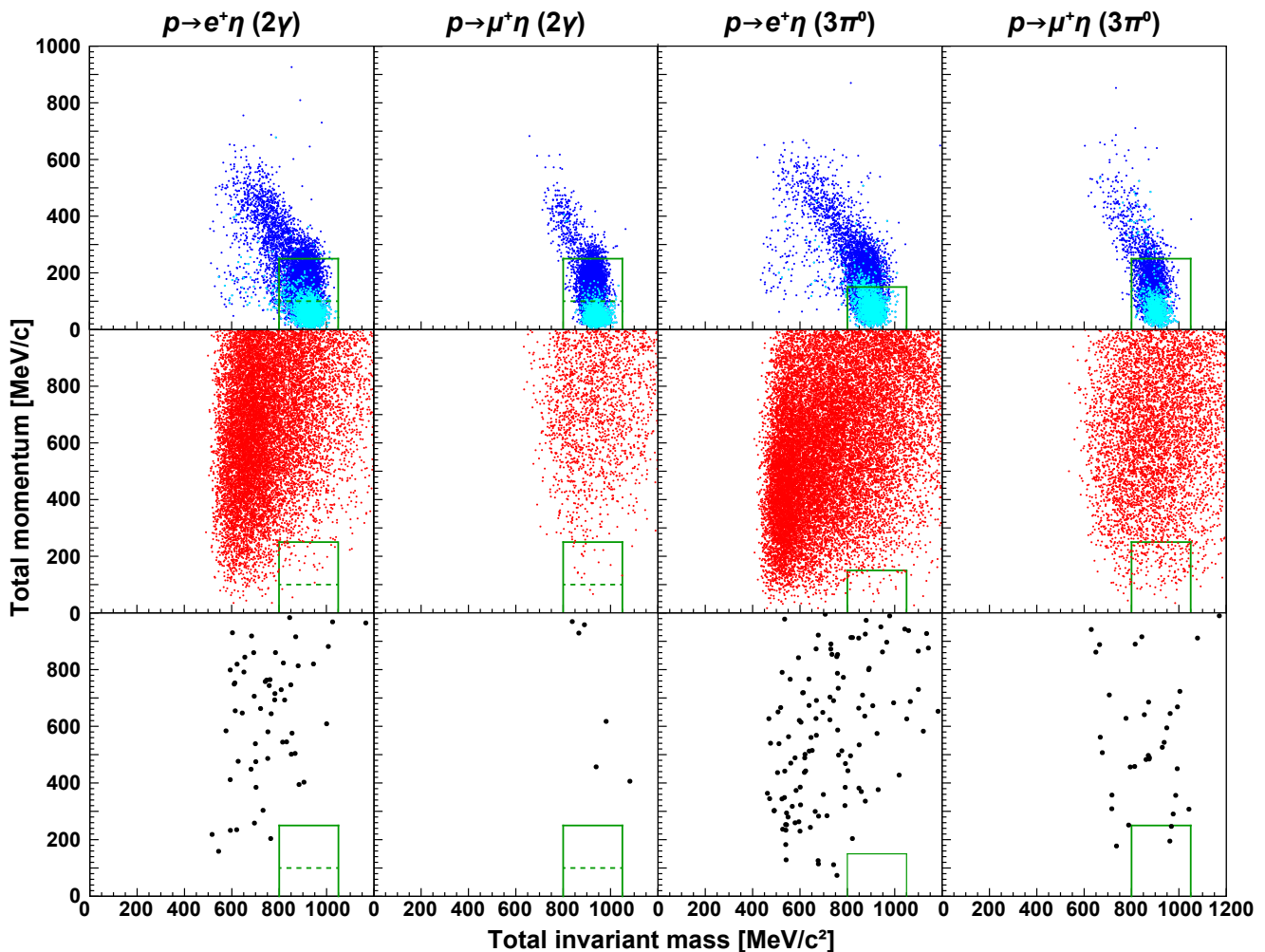


FIG. 4. Reconstructed total invariant mass and momentum of proton decay MC (upper), atmospheric neutrino MC (middle), and data (lower) for $p \rightarrow e^+ \eta$ ($\eta \rightarrow 2\gamma$), $p \rightarrow \mu^+ \eta$ ($\eta \rightarrow 2\gamma$), $p \rightarrow e^+ \eta$ ($\eta \rightarrow 3\pi^0$), $p \rightarrow \mu^+ \eta$ ($\eta \rightarrow 3\pi^0$) searches from left to right. The blue and cyan circles in the upper figures stand for bound and free proton decay events, respectively. The red circles in the middle and the black circles in the lower each correspond to the 500 years of atmospheric neutrino MC and the data from SK-I to SK-IV combined. The green solid and dashed lines indicate the selection criteria (A5-7) and (B5) in Section V. All the event selections except (A5-A7) and (B5) are applied.

butions and the one-dimensional distributions of the total mass and total momentum are shown in Figs. 4, 5, and 6, respectively. Unlike the $\eta \rightarrow 2\gamma$ search, a two-box separation in total momentum is not implemented here as a substantial fraction of events derived from free proton decays are reconstructed with total momenta greater than 100 MeV/c as shown in the upper figures in Fig. 6. A tighter cut on the total momentum of $P_{\text{tot}} < 150$ MeV/c at (B5) is applied for $p \rightarrow e^+ \eta$ mode to reduce backgrounds. The breakdown of the remaining background events by neutrino interaction mode is listed in Table II. Atmospheric neutrino events with neutral pions generating multiple showering rings dominate the background in both modes.

VI. SEARCH RESULTS

The search for proton decay was performed using 0.37 Mton · years of SK data by applying the selection criteria described in Section V. No signal candidate was found for the $p \rightarrow e^+ \eta$ mode whereas two events remain in the final signal region of the $\eta \rightarrow 3\pi^0$ decay search in the $p \rightarrow \mu^+ \eta$ mode. Both of the candidates are near the selection thresholds of the total mass and momentum cuts and are identical to those found in the previous analysis [11]. No significant data excess was found above the expected number of atmospheric neutrino background events in either mode. The total estimated background is 0.42 and 0.93 events for the $p \rightarrow e^+ \eta$ and $p \rightarrow \mu^+ \eta$ modes, respectively. The Poisson probability to observe

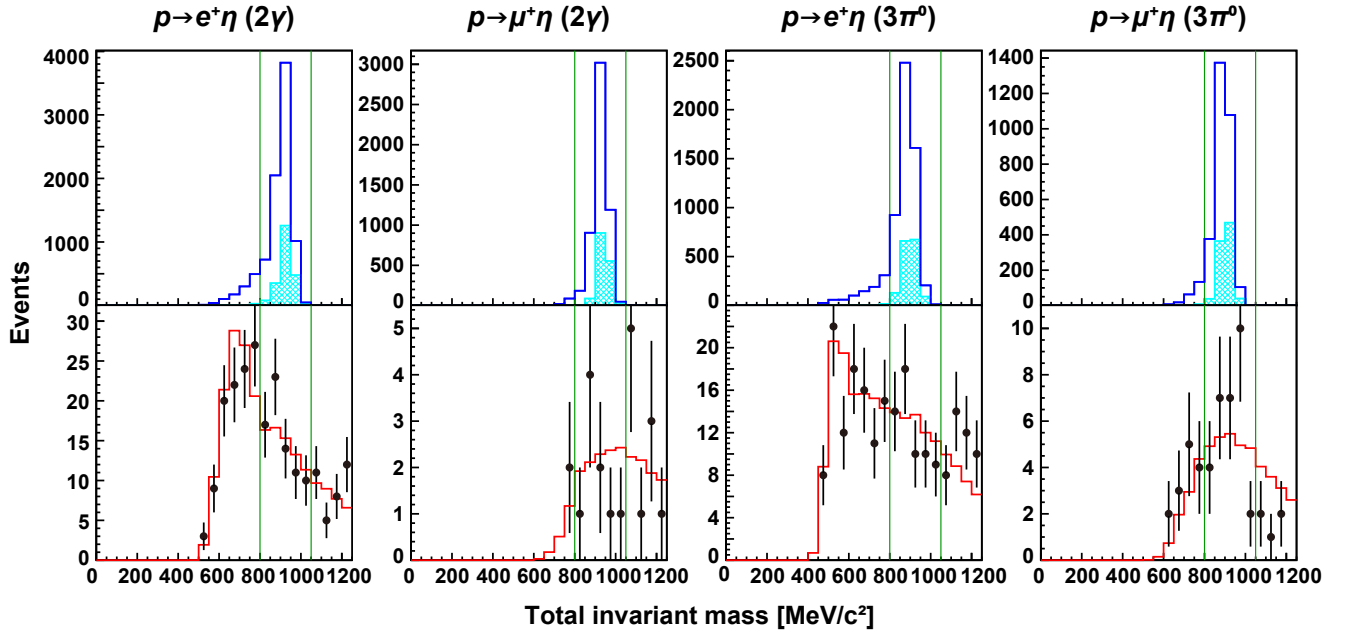


FIG. 5. Reconstructed total invariant mass of proton decay MC (upper), atmospheric neutrino MC and data (lower) for $p \rightarrow e^+ \eta (\eta \rightarrow 2\gamma)$, $p \rightarrow \mu^+ \eta (\eta \rightarrow 2\gamma)$, $p \rightarrow e^+ \eta (\eta \rightarrow 3\pi^0)$, $p \rightarrow \mu^+ \eta (\eta \rightarrow 3\pi^0)$ searches from left to right. The blue and cyan histograms in the upper figures stand for bound and free proton decay events, respectively. The red lines and the black circles in the lower each correspond to the 500 years of atmospheric neutrino MC and the data from SK-I to SK-IV combined. The green solid and dashed lines indicate the selection criteria (A5-7) and (B5) in Section V. All the event selections except (A5-A7) and (B5) are applied.

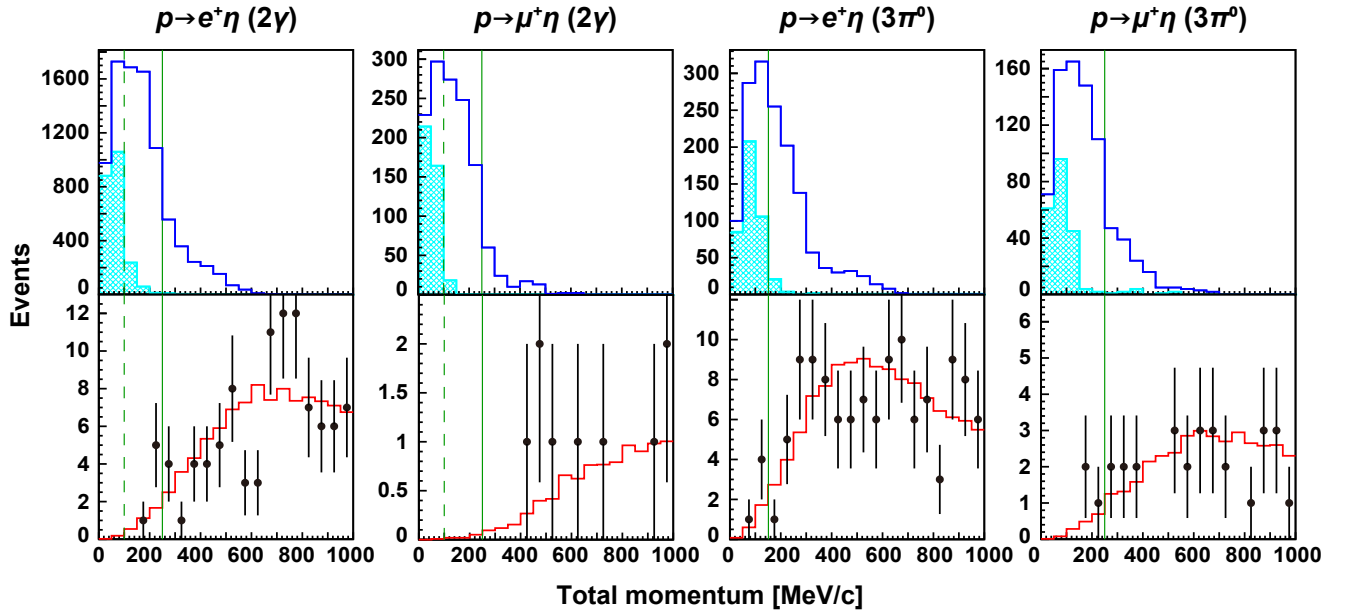


FIG. 6. Reconstructed total momentum of proton decay MC (upper), atmospheric neutrino MC and data (lower) for $p \rightarrow e^+ \eta (\eta \rightarrow 2\gamma)$, $p \rightarrow \mu^+ \eta (\eta \rightarrow 2\gamma)$, $p \rightarrow e^+ \eta (\eta \rightarrow 3\pi^0)$, $p \rightarrow \mu^+ \eta (\eta \rightarrow 3\pi^0)$ searches from left to right. The blue and cyan histograms in the upper figures stand for bound and free proton decay events, respectively. The red lines and the black circles in the lower each correspond to the 500 years of atmospheric neutrino MC and the data from SK-I to SK-IV combined. The green solid and dashed lines indicate the selection criteria (A5-7) and (B5) in Section V. All the event selections except (A5-A7) and (B5) are applied.

TABLE II. Breakdown (percentage contribution) of the neutrino interaction modes of the background events in the final signal boxes from SK-I to SK-IV in total. Here, CC and NC represent charged-current and neutral-current, respectively. QE, 1π , and multi π stand for quasielastic scattering, single π production and multiple π production, respectively.

| Interaction | $p \rightarrow e^+\eta$ | $p \rightarrow \mu^+\eta$ |
|-----------------|-------------------------|---------------------------|
| CCQE | 6 | 1 |
| CC 1π | 19 | 14 |
| CC multi π | 25 | 36 |
| CC & NC 1η | 6 | 11 |
| CC others | 7 | 8 |
| NC | 37 | 20 |

zero (two) or more events assuming mean values of 0.42 (0.93) is 65.7% (23.9%). As shown in Fig. 3, Fig. 5, and Fig. 6, the data and background MC are consistent both in the event rates along the event selection cuts and in the distributions of the relevant selection parameters.

A. Systematic Uncertainties

Systematic errors on the signal efficiencies and on the number of expected background events are summarized in Tables III and IV. Uncertainties from the physics modelling and event reconstruction performance are considered for both the proton decay signal and the atmospheric neutrino background MC. These systematic errors are estimated using the same methods as in the previous paper [11] except for those coming from η and π nuclear effects, as well as those from π secondary interactions in water for the background.

The systematic uncertainty arising from the η nuclear effect was the dominant error source for signal efficiency in the previous analysis [11]. In this study the uncertainty is estimated by varying the fitting parameters used to model σ_{nuc} within their $\pm 1\sigma$ errors (see Section III B) and propagating the altered cross section through the full analysis. The variation in the final signal efficiency relative to that from the nominal MC is adopted as the uncertainty. This new method provides a more reliable evaluation of systematic uncertainty from η nuclear interactions leading to a reduction in the associated error compared to the previous analysis, where the uncertainty in σ_{nuc} was evaluated by scaling the Breit Wigner function to cover all the measured data points in [19]. For the upper momentum box of the $\eta \rightarrow 2\gamma$ search, where the majority of the signal candidates derive from bound protons, this is a factor of three reduction. The error on the number of background events is taken as the variation in the event rate between MC generated with and without the updated nuclear effect cross section.

In the previous study, the π nuclear effect and secondary interaction uncertainties were considered to be independent and estimated separately. However, since

these two uncertainties have common error sources, they are now evaluated as a single error in this study. The current approach is identical to that adopted in the latest $p \rightarrow e^+\pi^0$ search at SK [5]. This improvement results in a reduction of the systematic error by at most $\sim 30\%$ compared to the previous $p \rightarrow l^+\eta$ analysis.

There are seven sources of uncertainty stemming from the event reconstruction: uncertainty in the vertex position, the number of Cherenkov rings, the particle identification (ring pattern), the number of Michel electrons, the energy scale, and the number of tagged neutrons for the SK-IV period. The same error estimation methods are applied for both the signal selection efficiencies and the number of expected background events. Due to limited MC statistics, the upper and lower signal boxes for the atmospheric neutrino background are combined when estimating the uncertainty. The resulting background error is then applied to both signal boxes.

B. Lifetime Limits

No significant event excess was observed in either decay mode and lower limits on the proton's partial lifetime are calculated using a Bayesian method [36, 37]. Lifetime limits are calculated by combining the 12 independent measurements for each $p \rightarrow l^+\eta$ mode: two (upper and lower) box analyses for $\eta \rightarrow 2\gamma$ and single signal box analysis for $\eta \rightarrow 3\pi^0$ taken over four different SK periods each.

The probability density function for each proton decay rate, Γ , is defined as

$$\mathbf{P}(\Gamma|n) = \frac{1}{A_i} \iiint \frac{e^{-(\Gamma\lambda_i\epsilon_i+b_i)} (\Gamma\lambda_i\epsilon_i + b_i)^{n_i}}{n_i!} \times \mathbf{P}(\Gamma)\mathbf{P}(\lambda_i)\mathbf{P}(\epsilon_i)\mathbf{P}(b_i)d\epsilon_i d\lambda_i db_i, \quad (4)$$

where i is the index of each measurement, n_i is the number of data candidates, λ_i is the detector exposure, ϵ is the signal selection efficiency, and b_i is the expected number of background events. The prior probability distribution on the decay rate $\mathbf{P}(\Gamma)$ is 1 for $\Gamma \geq 0$ and otherwise 0. $\mathbf{P}(\lambda_i)$, $\mathbf{P}(\epsilon_i)$, and $\mathbf{P}(b_i)$ stand for the prior probabilities for the detector exposure, signal efficiency, and number of background events, respectively, which are assumed to be Gaussian distributions:

$$\mathbf{P}(\lambda_i) \propto \begin{cases} \exp\left(-\frac{(\lambda_i - \lambda_{0i})^2}{2\sigma_{\lambda_i}^2}\right), & (\lambda_i > 0) \\ 0, & (\lambda_i \leq 0) \end{cases} \quad (5)$$

$$\mathbf{P}(\epsilon_i) \propto \begin{cases} \exp\left(-\frac{(\epsilon_i - \epsilon_{0i})^2}{2\sigma_{\epsilon_i}^2}\right), & (\epsilon_i > 0) \\ 0, & (\epsilon_i \leq 0) \end{cases} \quad (6)$$

TABLE III. Summary of the systematic uncertainties on signal efficiencies for each factor (in units of percent). The errors are averaged over SK-I to SK-IV periods by live time. The "upper" and "lower" in the $\eta \rightarrow 2\gamma$ searches stand for $100 \leq p_{\text{tot}} < 250$ MeV/c and $p_{\text{tot}} < 100$ MeV/c regions, respectively.

| Modes | η nuclear effect | N-N correlated decay | Fermi momentum | Event reconstruction | Total |
|----------------------------|-----------------------|----------------------|----------------|----------------------|-------|
| $p \rightarrow e^+ \eta$ | | | | | |
| (2γ , upper) | 9.1 | 9.6 | 6.0 | 4.6 | 14.7 |
| (2γ , lower) | 7.0 | 3.1 | 13.2 | 4.3 | 15.5 |
| ($3\pi^0$) | 6.6 | 5.1 | 15.5 | 3.7 | 17.9 |
| $p \rightarrow \mu^+ \eta$ | | | | | |
| (2γ , upper) | 8.4 | 9.8 | 7.5 | 3.6 | 15.6 |
| (2γ , lower) | 8.2 | 3.0 | 13.9 | 3.2 | 16.8 |
| ($3\pi^0$) | 9.4 | 6.8 | 2.9 | 6.1 | 13.8 |

TABLE IV. Summary of the systematic uncertainties on the number of background events for each factor (in units of percent). The errors are averaged over SK-I to SK-IV periods by live time. The "upper" and "lower" in the $\eta \rightarrow 2\gamma$ searches stand for $100 \leq p_{\text{tot}} < 250$ MeV/c and $p_{\text{tot}} < 100$ MeV/c regions, respectively.

| Modes | Neutrino flux | Neutrino cross section | π interaction | η nuclear effect | Event reconstruction | Total |
|----------------------------|---------------|------------------------|-------------------|-----------------------|----------------------|-------|
| $p \rightarrow e^+ \eta$ | | | | | | |
| (2γ , upper) | 8.5 | 15.6 | 8.9 | 3.0 | 24.1 | 31.6 |
| (2γ , lower) | 8.8 | 14.9 | 13.2 | 1.0 | 18.8 | 28.9 |
| ($3\pi^0$) | | | | | | |
| $p \rightarrow \mu^+ \eta$ | | | | | | |
| (2γ , upper) | 9.3 | 20.6 | 14.9 | 3.0 | 29.1 | 39.9 |
| (2γ , lower) | 8.8 | 10.4 | 15.7 | 1.0 | 10.2 | 23.0 |
| ($3\pi^0$) | | | | | | |

Here λ_{0i} (σ_{λ_i}) and ϵ_{0i} (σ_{ϵ_i}) are nuisance parameters for the exposure and signal efficiency (their uncertainties). The uncertainties on the detector exposures are assumed to be less than 1%. As the number of background events b_i is low enough, a convolution of Poisson and Gaussian distribution is adopted for the probability of the number of background to take into account the MC statistical error. Therefore, $\mathbf{P}(b)$ is expressed as

$$\mathbf{P}(b_i) \propto \begin{cases} \int_0^\infty \frac{e^{-B}(B)^{n_{b_i}}}{n_{b_i}!} \\ \times \exp\left(-\frac{(b_i C_i - B)^2}{2\sigma_{b_i}^2}\right) dB, & (b_i > 0) \\ 0. & (b_i \leq 0) \end{cases} \quad (7)$$

Here n_{b_i} is the expected number of background events in 500 years of atmospheric neutrino MC, B is the number of true background events in 500 years of atmospheric neutrino MC, C_i is the normalization constant for MC live time to the data live time, and σ_{b_i} is the systematic error of the number of background events. With these definitions, the lower limit on the proton decay rate for the full search, Γ_{limit} , at a given C.L. is

$$\text{C.L.} = \int_0^{\Gamma_{\text{limit}}} \prod_{i=1}^{12} \mathbf{P}_i(\Gamma|n_i) d\Gamma, \quad (8)$$

TABLE V. Summary of proton decay search of $p \rightarrow l^+ \eta$.

| Modes | Background [events] | Candidate [events] | Probability [%] | Lifetime limit at 90% CL |
|----------------------------|---------------------|--------------------|-----------------|---------------------------|
| $p \rightarrow e^+ \eta$ | 0.42 ± 0.13 | 0 | 65.7 | 1.4×10^{34} yrs. |
| $p \rightarrow \mu^+ \eta$ | 0.93 ± 0.25 | 2 | 23.9 | 7.3×10^{33} yrs. |

with the lower lifetime limit defined as:

$$\tau/B = \frac{1}{\Gamma_{\text{limit}}}. \quad (9)$$

The lifetime limits at 90% C.L. are $\tau/B(p \rightarrow e^+ \eta) > 1.4 \times 10^{34}$ years and $\tau/B(p \rightarrow \mu^+ \eta) > 7.3 \times 10^{33}$ years. Both limits have increased by a factor of 1.5 relative to the previous analysis. This increase is attributed to both the newly analysed SK-IV data (55.7 kton-years) which corresponds to a $\sim 18\%$ increase in the total exposure and to the revised η nuclear effect, which has improved the signal efficiency and reduced associated systematic errors. The results of these searches are summarized in Table V.

VII. CONCLUSION

Searches for proton decay into a charged antilepton and an η meson were performed with an updated nuclear effect estimation and with an additional 55.7 kton-years of SK-IV data since the last analysis [11]. The updated nuclear effect led to improvements both in signal efficiency ($\sim 10\%$) and a reduction in this previously dominantly systematic uncertainty (a factor of three). Using a combined exposure of 0.37 Mton \cdot years, the number of candidate events was consistent with the atmospheric neutrino background prediction and no indication of proton decay was observed for either mode. Lower limits on the partial proton lifetime of 1.4×10^{34} years for $p \rightarrow e^+ \eta$ and 7.3×10^{33} years for $p \rightarrow \mu^+ \eta$ are set at 90% C.L. These limits are around 1.5 times longer than our previous study and are the most stringent to date.

ACKNOWLEDGMENTS

We gratefully acknowledge the cooperation of the Kamioka Mining and Smelting Company. The Super-Kamiokande experiment has been built and operated from funding by the Japanese Ministry of Education, Culture, Sports, Science and Technology; the U.S. Department of Energy; and the U.S. National Sci-

ence Foundation. Some of us have been supported by funds from the National Research Foundation of Korea (NRF-2009-0083526, NRF-2022R1A5A1030700, NRF-2202R1A3B1078756) funded by the Ministry of Science, Information and Communication Technology (ICT); the Institute for Basic Science (IBS-R016-Y2); and the Ministry of Education (2018R1D1A1B07049158, 2021R1I1A1A01042256, 2021R1I1A1A01059559); the Japan Society for the Promotion of Science; the National Natural Science Foundation of China under Grants No.12375100; the Spanish Ministry of Science, Universities and Innovation (grant PID2021-124050NB-C31); the Natural Sciences and Engineering Research Council (NSERC) of Canada; the Scinet and Westgrid consortia of Compute Canada; the National Science Centre (UMO-2018/30/E/ST2/00441 and UMO-2022/46/E/ST2/00336) and the Ministry of Science and Higher Education (2023/WK/04), Poland; the Science and Technology Facilities Council (STFC) and Grid for Particle Physics (GridPP), UK; the European Union's Horizon 2020 Research and Innovation Programme under the Marie Skłodowska-Curie grant agreement no.754496; H2020-MSCA-RISE-2018 JENNIFER2 grant agreement no.822070, H2020-MSCA-RISE-2019 SK2HK grant agreement no. 872549; and European Union's Next Generation EU/PRTR grant CA3/RSUE2021-00559; the National Institute for Nuclear Physics (INFN), Italy.

-
- [1] H. Georgi and S. L. Glashow, Unity of all elementary-particle forces, *Phys. Rev. Lett.* **32**, 438 (1974).
- [2] H. Fritzsch and P. Minkowski, Unified interactions of leptons and hadrons, *Ann. Phys. (N. Y.)* **93**, 193 (1975).
- [3] N. Sakai and T. Yanagida, Proton decay in a class of supersymmetric grand unified models, *Nucl. Phys. B* **197**, 533 (1982).
- [4] S. Weinberg, Supersymmetry at ordinary energies. Masses and conservation laws, *Phys. Rev. D* **26**, 287 (1982).
- [5] A. Takenaka *et al.* (The Super-Kamiokande Collaboration), Search for proton decay via $p \rightarrow e^+ \pi^0$ and $p \rightarrow \mu^+ \pi^0$ with an enlarged fiducial volume in Super-Kamiokande I-IV, *Phys. Rev. D* **102**, 112011 (2020).
- [6] K. Abe *et al.* (The Super-Kamiokande Collaboration), Search for nucleon decay via $n \rightarrow \bar{\nu} \pi^0$ and $p \rightarrow \bar{\nu} \pi^+$ in super-kamiokande, *Phys. Rev. D* **113**, 1 (2014).
- [7] M. Machacek, The decay modes of the proton, *Nucl. Phys. B* **159**, 37 (1979).
- [8] M. B. Gavela, A. Le Yaouanc, L. Oliver, O. Pène, and J. C. Raynal, Exclusive modes of proton decay in SU(5), *Phys. Lett. B* **98**, 51 (1981).
- [9] J. F. Donoghue, Proton lifetime and branching ratios in SU(5), *Phys. Lett. B* **92**, 99 (1980).
- [10] F. Buccella, G. Miele, L. Rosa, P. Santorelli, and T. Tuzi, An upper limit for the proton lifetime in SO(10), *Phys. Lett. B* **233**, 178 (1989).
- [11] K. Abe *et al.* (The Super-Kamiokande Collaboration), Search for nucleon decay into charged antilepton plus meson in 0.316 megaton-years exposure of the Super-Kamiokande water Cherenkov detector, *Phys. Rev. D* **96**, 1 (2017).
- [12] S. Fukuda *et al.* (The Super-Kamiokande Collaboration), The Super-Kamiokande detector, *Nucl. Instr. Meth. A* **501**, 418 (2003).
- [13] K. Abe *et al.* (The Super-Kamiokande Collaboration), Calibration of the Super-Kamiokande detector, *Nucl. Instr. Meth. A* **747**, 253 (2014).
- [14] H. Nishino, K. Awai, Y. Hayato, S. Nakayama, K. Okumura, M. Shiozawa, A. Takeda, K. Ishikawa, A. Minegishi, and Y. Arai, High-speed charge-to-time converter ASIC for the Super-Kamiokande detector, *Nucl. Instr. Meth. A* **610**, 710 (2009).
- [15] R. D. Woods and D. S. Saxon, Diffuse surface optical model for nucleon-nuclei scattering, *Phys. Rev.* **95**, 577 (1954).
- [16] K. Nakamura, S. Hiramatsu, T. Kamae, H. Muramatsu, N. Izutsu, and Y. Watase, The reaction $^{12}\text{C}(e, e'p)$ at 700 MeV and DWIA analysis, *Nucl. Phys. A* **268**, 381 (1976).
- [17] T. Yamazaki and Y. Akaishi, *Phys. Lett. B* **453**, 1 (1999).
- [18] B. Krusche and C. Wilkin, Production of η and η' mesons on nucleons and nuclei, *Prog. Part. Nucl. Phys.* **80**, 43 (2015).
- [19] M. Rößig-Landau, J. Ahrens, G. Anton, R. Averbeck, R. Beck, M. Fuchs, A. Gabler, F. Härter, P. Harty, V. Hejny, *et al.*, Near threshold photoproduction of η -mesons from complex nuclei, *Phys. Lett. B* **373**, 45 (1996).
- [20] H. Nishino *et al.* (The Super-Kamiokande Collaboration), Search for nucleon decay into charged antilepton plus me-

- son in Super-Kamiokande I and II, *Phys. Rev. D* **85**, 112001 (2012).
- [21] G. Breit and E. Wigner, Capture of Slow Neutrons, *Phys. Rev.* **49**, 519 (1936).
- [22] Y. Hayato, NEUT, *Nucl. Phys. Proc. Suppl.* **112**, 171 (2002).
- [23] Y. Hayato, A neutrino interaction simulation program library NEUT, *Acta Phys. Pol. B* **40**, 2477 (2009).
- [24] M. Honda, T. Kajita, K. Kasahara, S. Midorikawa, and T. Sanuki, Calculation of atmospheric neutrino flux using the interaction model calibrated with atmospheric muon data, *Phys. Rev. D* **75**, 1 (2007).
- [25] M. Honda, T. Kajita, K. Kasahara, and S. Midorikawa, Improvement of low energy atmospheric neutrino flux calculation using the JAM nuclear interaction model, *Phys. Rev. D* **83**, 1 (2011).
- [26] K. Abe *et al.* (The Super-Kamiokande Collaboration), Atmospheric neutrino oscillation analysis with external constraints in Super-Kamiokande I-IV, *Phys. Rev. D* **97**, 72001 (2018).
- [27] L. Salcedo, E. Oset, M. Vicente-Vacas, and C. Garcia-Recio, Computer simulation of inclusive pion nuclear reactions, *Nucl. Phys. A* **484**, 557 (1988).
- [28] P. de Perio, S. K. Singh, J. G. Morfin, M. Sakuda, and K. D. Purohit, NEUT Pion FSI, in *AIP Conf. Proc.*, Vol. 1405 (2011) pp. 223–228.
- [29] D. Rein and L. M. Sehgal, Neutrino-excitation of baryon resonances and single pion production, *Ann. Phys. (N. Y.)* **133**, 79 (1981).
- [30] M. Shiozawa, Reconstruction algorithms in the Super-Kamiokande large water Cherenkov detector, *Nucl. Instr. Meth. A* **433**, 240 (1999).
- [31] A. Takenaka, Ph.D. thesis, The University of Tokyo (2020).
- [32] E. R. Davies, *Machine Vision: Theory, Algorithms, Practicalities* (Academic Press, San Diego, 1997).
- [33] K. Abe *et al.* (The Super-Kamiokande Collaboration), Neutron tagging following atmospheric neutrino events in a water Cherenkov detector, *JNIST* **17**, 40 (2022).
- [34] M. Tanaka *et al.* (The Super-Kamiokande Collaboration), Search for proton decay into three charged leptons in 0.37 megaton-years exposure of the Super-Kamiokande, *Phys. Rev. D* **101**, 52011 (2020).
- [35] H. Ejiri, Nuclear deexcitations of nucleon holes associated with nucleon decays in nuclei, *Phys. Rev. C* **48**, 1442 (1993).
- [36] C. Amsler *et al.* (Particle Data Group Collaboration), Review of Particle Physics, *Phys. Lett. B* **667**, 1 (2008).
- [37] B. P. Roe and M. B. Woodroffe, Setting confidence belts, *Phys. Rev. D* **63**, 13009 (2000).